

# 2nd Aide mémoire for g-mode search

B.Andersen, T.Appourchaux, W.Chaplin, Y.Elsworth,  
W.Finsterle, C.Fröhlich, D.O.Gough, G.Isaak,  
J.Provost, T.Toutain, T.Sekii & P.Scherrer

May 12, 1999

## Abstract

This aide mémoire summarizes the joint effort of the SOI/MDI, BiSON and VIRGO team for discovering g modes. The data sets and their reduction are described. The different technique used for detecting g modes are described. A list of g- and p-mode frequencies are given for 2 different models. This aide mémoire shall be used as a basis for writing papers on g-mode upper limit, g-mode detection techniques and low frequency p-mode detection.

*It is superficially unfortunate that we discovered no g modes. On the brighter side, on which I always prefer to be, it shows that we have before us a greater challenge which will yield [ ] greater satisfaction when we overcome it[...]. We are all now much more prepared to continue the search.*

*Douglas Gough, December 1997*

## 1 Foreword

In the course of the development of the Phoebus workshops, it became obvious during the 2nd workshop that we would need slightly more time to detect g modes. The Boston meeting exemplified this fact by giving a detection time of 20 years (Fröhlich et al., 1998). During the last workshop we had 3 items on our paper production agenda:

- upper limit of g-mode amplitude
- low frequency p-mode detection
- g-mode detection technique

Of the three, the last item was not really discussed as it is still an ongoing activity. The success of which would lie in the detection of of at least a pair of g modes. The aide mémoire shows clearly the fragile status of some of the detection techniques.

The first two items in terms of writing papers are still high on our agenda. Two papers were published at the Boston meeting on this subject. Some time since then has been wasted due to the physical condition of the secretary of the group. During the week on May 7, 1999, W.Chaplin, D.Gough and T.Appourchaux had a discussion on the writing of such papers. We agreed that the writing of a paper on the upper limit of g-mode amplitude would be timely and for which most of the work has already been performed.

The other paper on low frequency p modes may need some additional work as it is rather clear that time will improve our detection limit and that we would also benefit from the development of g-mode detection techniques.

## 2 Introduction

The aide mémoire is made of 3 sections. The first section describes the data utilized. This section is almost completed and may require some additional tuning to be used as such. The second section is about the g-mode detection strategies. This section is still being worked and so are the strategies; obviously only part of it could be useful in the eventuality of writing an article on the subject. The last section is about the p-mode amplitude and noise levels. This section is mainly a description of the way the data are calibrated to get the proper limit on g-mode amplitude. This would not probably go directly into the paper. As a matter of fact, we already published a paper for the Boston meeting without this preliminary work.

## 3 Data utilized

### 3.1 SOI/MDI velocity

MDI dataset is the level-1.4 LOI velocity proxy (180 pixels) from 1 May 1996 to 24 June 1998 (784 days). Data with bad quality flag are put to 0. They are corrected from the satellite velocity and the offset due to tuning of the MDI. Then they are detrended using a third order polynomial. This is done in-between two changes of offset separately for each piece of signal. An  $(l, m)$  spherical harmonic mask with  $B = 0$  is applied to the data the resulting timeseries is high-pass filtered using a box-car smooth with a 1-day width. Data are then Fourier transformed.

### 3.2 VIRGO/SPM

The SPM data are based on the level 1 time series from 23 May 1996 and ends on 31 December 1997 (588 days). A running mean detrending of triangular shape and base width of two days was applied before computing the Fourier transform.

### 3.3 VIRGO/PMO6

The PMO6 data are based on the level 1 time series from 23 May 1996 and ends on 31 December 1997 (588 days). A running mean detrending of triangular shape and base width of two days was applied before computing the Fourier transform.

### 3.4 VIRGO/LOI

The LOI data are the level 1 data as reduced per VIR-SSD-GSE/L-001, (Ver 1.7, May 1996) from the level 0 data. It is available from the VIRGO home page. The LOI data are reduced in the same way as the SOI/MDI data except that there is no need to remove the 12-pixel average. The time series starts on 1 May 1996 to 24 June 1998 (784 days).

### 3.5 BiSON

The BiSON time series starts on 23 May 1996 and ends on 31 December 1997 (588 days). Two time series were available optimized either for g-mode or p-mode detection.

### 3.6 GONG

The GONG data time series start on 7 May 1995 and is 1080-day long. The time series was generated for  $l = 1, 2$  and 3.

## 4 g-mode finding strategies

### 4.1 Patterns techniques and collapsogrammes

All the pattern techniques assume that the g modes are splitted by rotation and/or that their frequencies are derived from an asymptotic formula (Fröhlich and Andersen, 1995; Fröhlich and Delache, 1984). In order for these techniques to be efficient, it is required that the splitted modes be present. Unfortunately, it can happen that, due to beating with the noise, the modes do not appear. As an example, Fig. 1 shows that sometimes not all of the components of a p-mode multiplet are ‘excited’. As a matter of fact, the modes are always excited but since the low-frequency p modes have a low amplitude they beat with the noise; sometimes the noise enhances the mode or suppresses it. Figure 2 shows a simulation for 140 days of data of such a beating. This very simple simulation means that the detection of a ‘g-mode peak’ in one time series may not be confirmed by another independent time series. A proper statistical analysis of many independent time series would be needed before confirming the detection of a g mode.

Keeping the statistical behaviour of the multiplet in mind, we have nevertheless devised a new pattern technique for detecting g modes: *the collapsogramme*. Each  $m$  spectrum is shifted from the  $m = 0$  spectrum by  $m\Omega$  (where  $\Omega$  represents the splitting of the mode), then each spectrum is normalized by an estimate of the variance of the spectrum, and finally the  $2l+1$  spectra are added together. The advantage of this technique is that it gets rid of the instrumental harmonics (invariant), and produces a spectrum

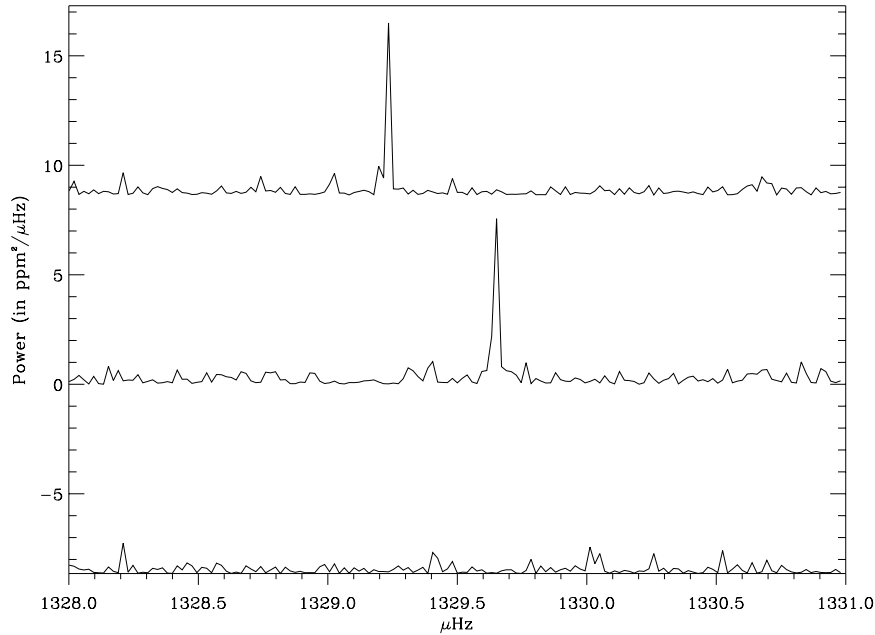


Figure 1:  $(m, \nu)$  diagram for the  $l = 1$ ,  $n = 8$  as observed by SOI/MDI. The frequency resolution is about 19nHz (610 days of data). The power spectra from top to bottom are for  $m = +1$ ,  $m = 0$  and  $m = -1$ , respectively.

with a well defined statistics (nearly a  $\chi^2$  with  $4l + 2$  d.o.f.). The disadvantage is that the g-mode splitting varies faster with frequency than for the p modes; the technique should be restricted to frequency band where the splitting varies slowly. Figures 3 and 4 show collapsogrammes in the p-mode frequency range for  $l = 1$  and  $l = 6$ , respectively. Lower-frequency p modes can be detected showing the efficiency of the technique. Results by the Phoebus group using this technique on low frequency p modes can be found in the SOHO6 proceedings (Appourchaux et al, 1998).

Using the GONG data, the collapsogram proved to be useful as Rabello-Soares and Appourchaux (1999) (A&A, in press) were able to go to lower frequencies that is currently possible with conventional fitting techniques (around 1400  $\mu\text{Hz}$  with a 1-year time series). At the time of the 2nd workshop, we could go even lower close to 1250  $\mu\text{Hz}$ .

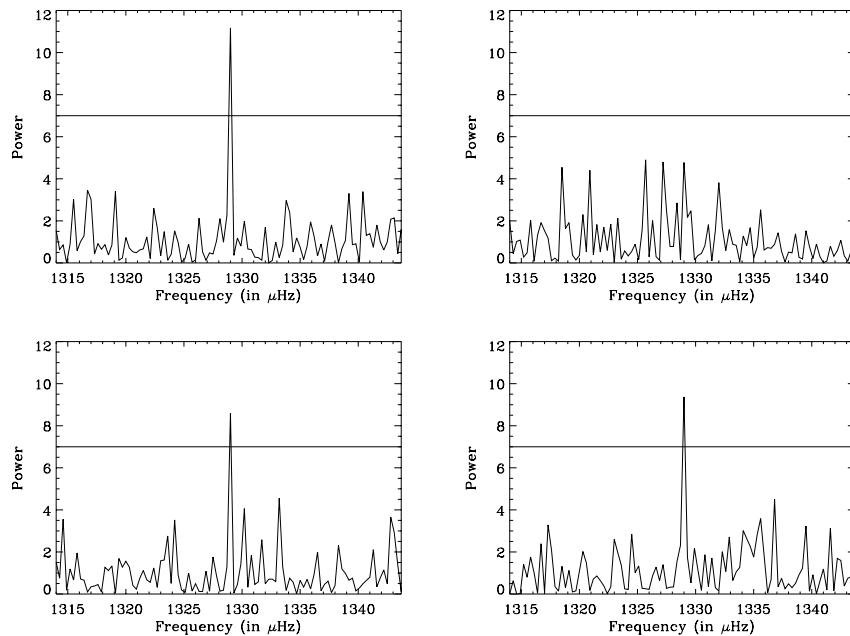


Figure 2: Simulated  $l = 1$ ,  $n = 8$  with a signal-to-noise ratio of 6.25 in the power spectrum. The resolution is about 80 nHz. The mean statistical probability that the mode be higher than  $7 \sigma$  is about 2 chances over 3.

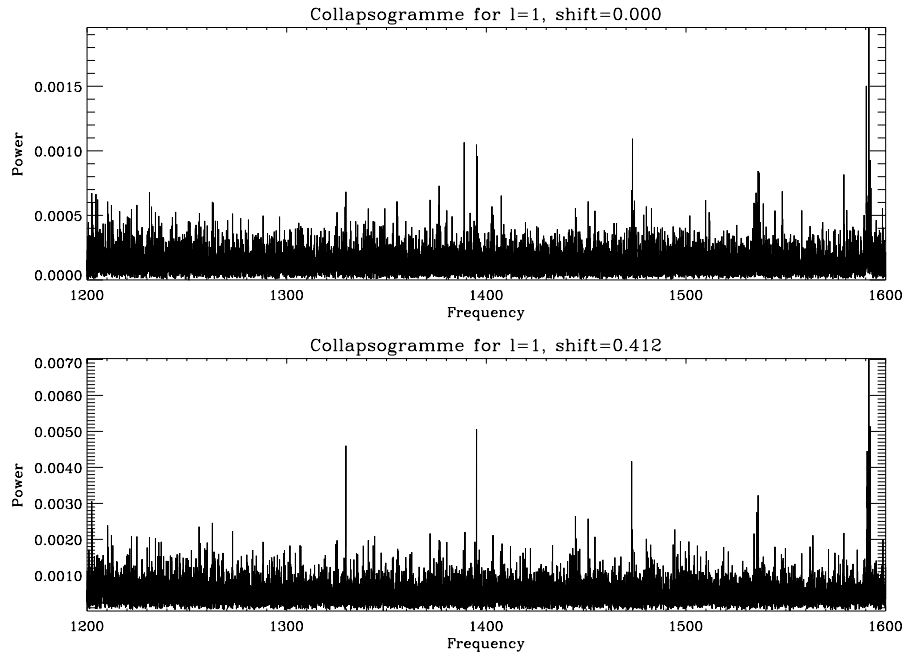


Figure 3: Collapsogramme for 610 days of SOI/MDI data for  $l = 1$ . Top: unshifted; bottom: shifted by 412 nHz. The  $n = 8, l = 1$  mode gets out better in the shifted collapsogramme, as expected.

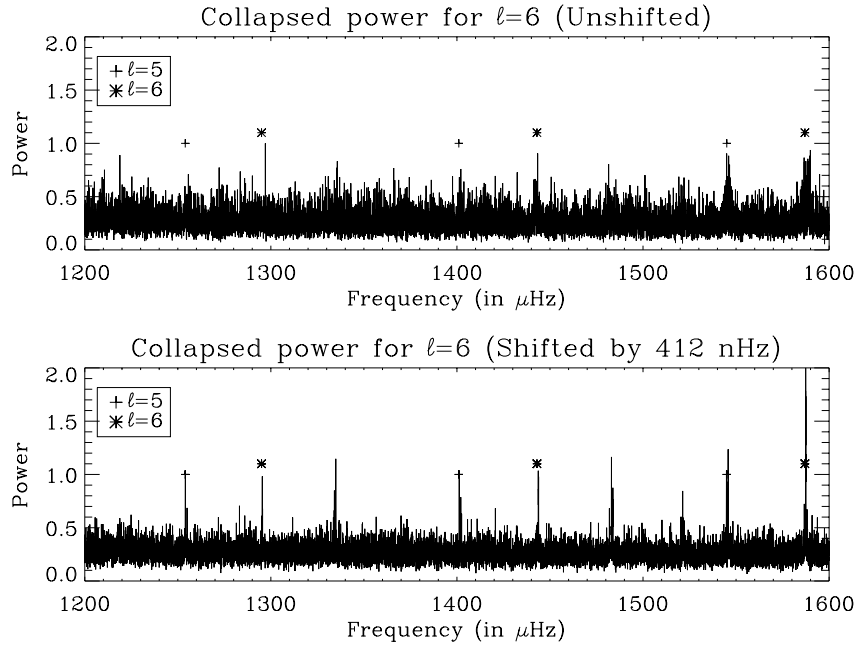


Figure 4: Collapsogramme for 610 days of SOI/MDI data for  $l = 6$ . Top: unshifted; bottom: shifted by 412 nHz.

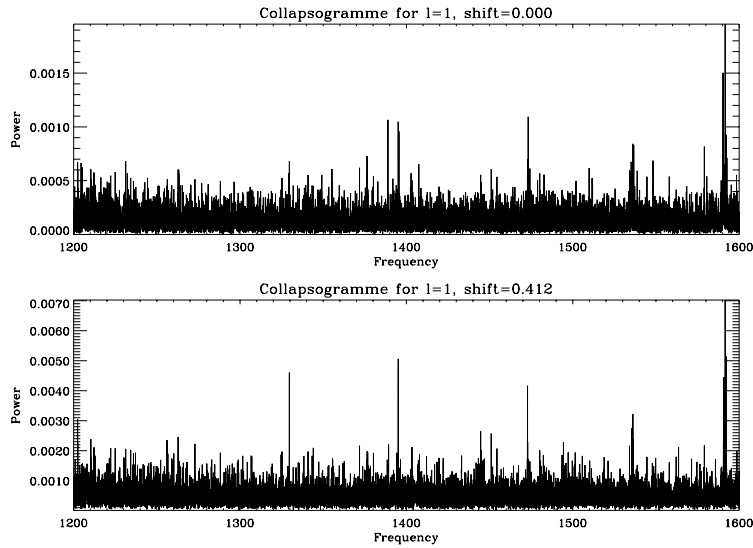


Figure 5: The central peak is an  $l = 2$ ,  $n = 8$ . The 2 peaks on either side are  $l = 1$ ,  $n = 8, 9$ .

## 4.2 Collapsoimage

The collapsoimage is technique derived from the collapsogramme. It is very often useful to visualize the collapsogramme obtained for each splitting. By scanning through a range of reasonable splittings, e.g. from 0 to 1  $\mu\text{Hz}$ , one can obtain a 2-D image of the collapsogramme, i.e. a collapsoimage.

## 4.3 Overlapogram

The principle of the overlapogram is similar to that of the collapsogram. Instead only one power spectrum is used and shifted from itself. This technique is mainly used by full-disk integrating instruments having only one power spectrum at their disposal.

## 4.4 Phase analysis

This part to be written by Wolfgang Finsterle.

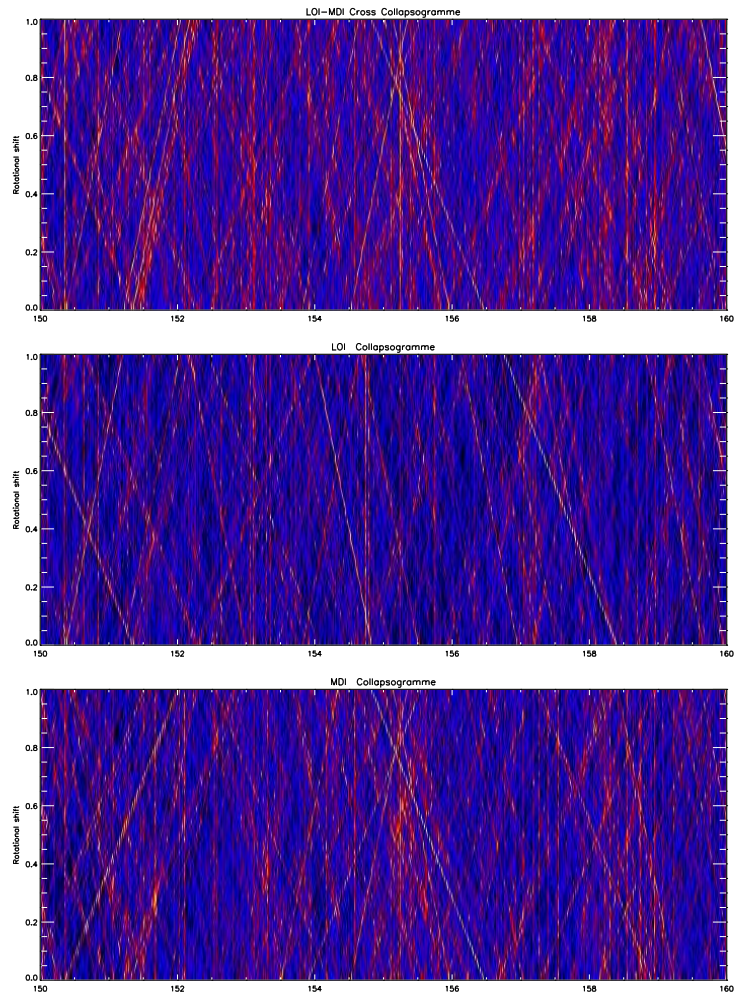


Figure 6: Collapseimage for LOI, MDI power spectra and for the LOI-MDI cross spectrum

## 4.5 On Bayesian approach

The so-called Bayesian approach is yet to be worked out. The purpose of this approach would be to help us detect additional p modes, and of course g

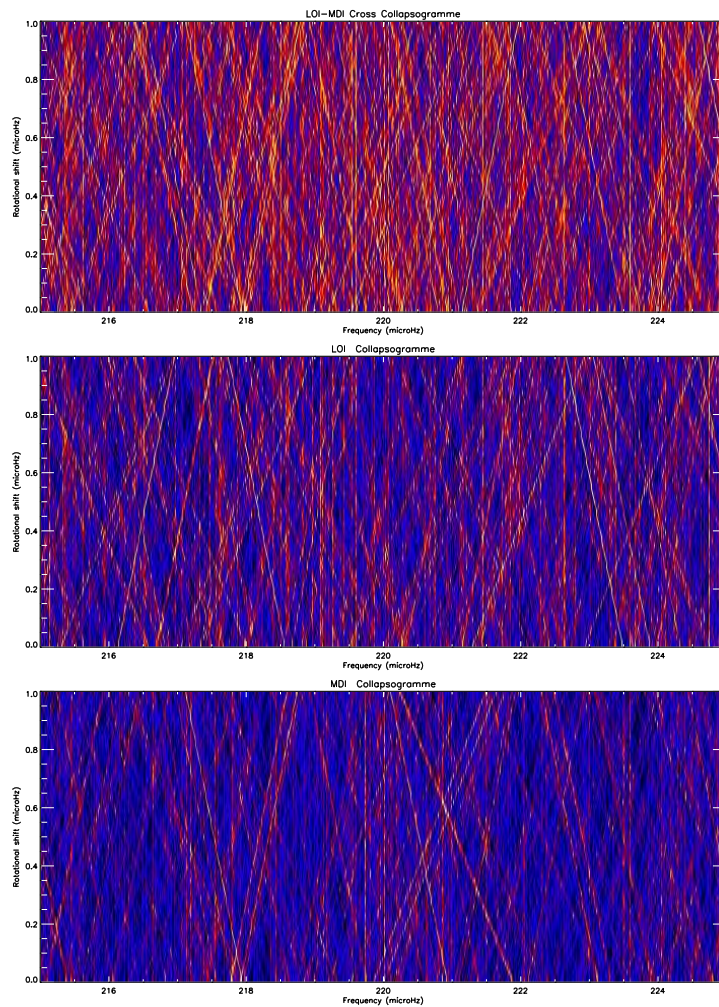


Figure 7: Collapseimage for LOI, MDI power spectra and for the LOI-MDI cross spectrum

modes. In the framework of writing an article on the upper limit of g modes, they may be procrastinated to the next workshop anyway.

## 4.6 Line-crossing probability

The collapse image is a visual guide for seeking uniformly spaced peaks in a power spectrum or a cross-correlation spectrum. To date it is being used for *uniform* spacing (which is what rotational splitting would be were the angular velocity of the Sun to be a function only of radius and if there is no asphericity in the seismic structure), but it can evidently be generalized to any given relative separation of peaks in a multiplet spectrum. The analysis presented below would be essentially unchanged in the generalized case, so for simplicity I use the language for the case of uniform spacing.

For dipole modes one has three components: in the collapse image the modes with  $m = \pm 1$  are equally (in magnitude) inclined (but in opposite direction) and  $m = 0$  is vertical. The collapse image is an excellent *device* for spotting uniformly spaced triplets, because the signature is three lines meeting at a point. What is the probability of this occurring at random?

The vertical extent  $\Delta\nu$  (or splitting range) of the collapse image is, in the case of our example,  $1 \mu\text{Hz} = 1000 \text{ nHz}$ . Any two lines inclined in opposite senses and with frequencies differing by less than  $2000 \text{ nHz}$  are bound to cross somewhere in the vertical range. Therefore, the only question to ask is : what is the probability that a vertical line will pass within some tolerance  $w$  of all such intersections in a collapse image?

Let the mean density of positively inclined lines be  $n$  per  $1000 \text{ nHz}$  interval. The distribution is assumed to be random, with uniform probability density. For simplicity I assume that the mean density of negatively inclined lines is the same (this seems to be borne out by observation). Then the density of intersections is  $n^2$ , and is also uniformly distributed. If the vertical lines are also uniformly distributed, with density  $N$  per  $1000 \text{ nHz}$ , then the probability  $p_{cross}$  of there being no intersection within the tolerance  $w$  in a  $1000 \text{ nHz}$  interval is:

$$p_{cross} = e^{-n^2 N w / \Delta\nu} \quad (1)$$

The horizontal extent of a collapse image is  $5000 \text{ nHz}$  ( $=5 \Delta\nu$ ). Suppose also we accept as ‘reasonable’ only splittings in a range  $\alpha\Delta\nu$  — Takashi suggests starting with  $\alpha=0.2$  — then the probability of at least one intersection of 3 lines within the tolerance is

$$P_1 = 1 - e^{-5\alpha n^2 N w / \Delta\nu} \quad (2)$$

From typical diagrams,  $n$  and  $N$  are not uniform, but the values  $n = N=5$  are not atypical. In that case:

$$P_1 = 1 - e^{-0.125w} \quad (3)$$

For a year of observation one might set  $w=30$  (some might say 45), Then  $P_1 = 1 - e^{-3.75}=0.98$ . Thus, it is extremely likely that a diagram with pure noise has at least one intersection of three lines.

In the case of a quadruple mode, with 5 lines, we need to calculate the probability that, in addition, two lines with half the slope also intersect within the tolerance. If the density of  $m = \pm 2$  is also  $n$  per  $\Delta\nu$ , the probability of three being no intersections of the five lines is:

$$P_{cross} = e^{-5\alpha n^3 N w^2 / (\Delta\nu)^2} \quad (4)$$

with the same parameters as before, the probability of at least one intersection of 5 randomly distributed in a collapse image is  $P_2 = 1 - e^{-0.56}=0.43$ .

The conclusion is that although the collapse image provides a good visual aid for finding mode candidates, on its own it is *not* a means of identifying modes.

## 4.7 Effect of core rotation on g-mode splittings

Figures 8 to 10 are results that were left on the `homefred` directory of Janine. The figures represent the effect of various core rotation: 433, 866 and 1732 nHz, with a core radius  $0.2R_\odot$  (TBC). These kind of information is useful when we will detect g modes in various frequency bands. I would appreciate that Janine give me slightly more information on how these splittings were obtained.

# 5 low-order p modes

## 5.1 Improvement in solar internal structure

A short note should be written by D.Gough on this subject.

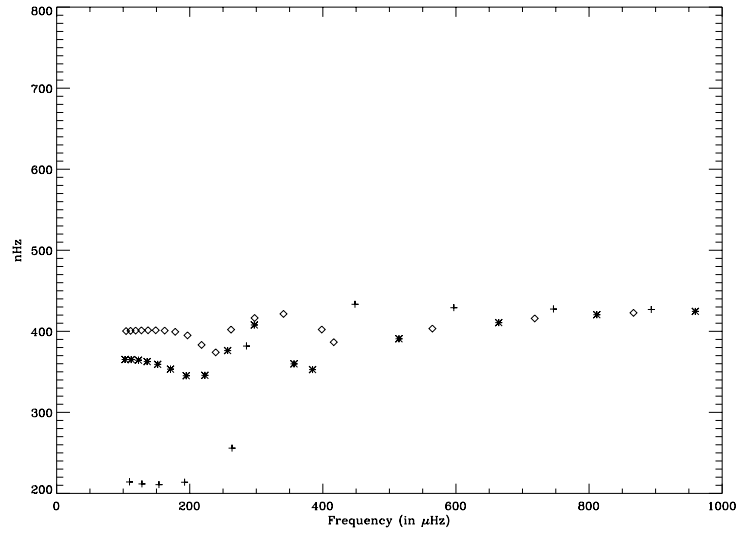


Figure 8: Splitting as a function of frequency for different degree (plus  $l = 1$ , star  $l = 2$ , diamond  $l = 3$ . Core rotation is 433 nHz.

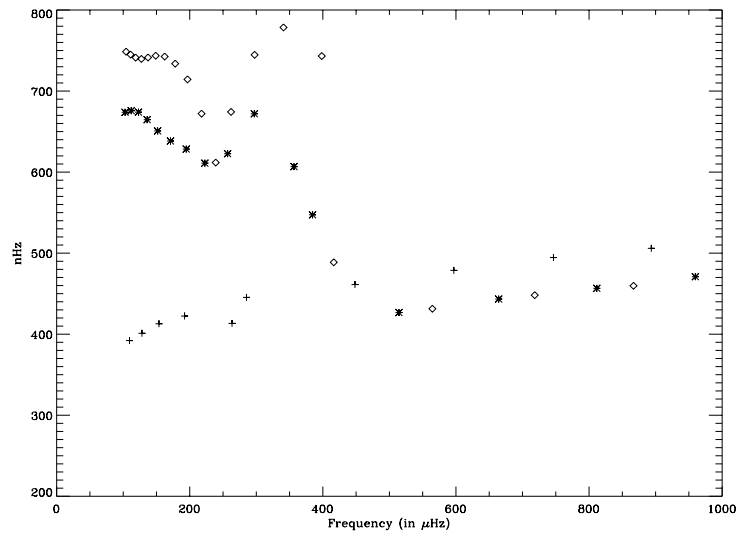


Figure 9: Splitting as a function of frequency for different degree (plus  $l = 1$ , star  $l = 2$ , diamond  $l = 3$ . Core rotation is 866 nHz.

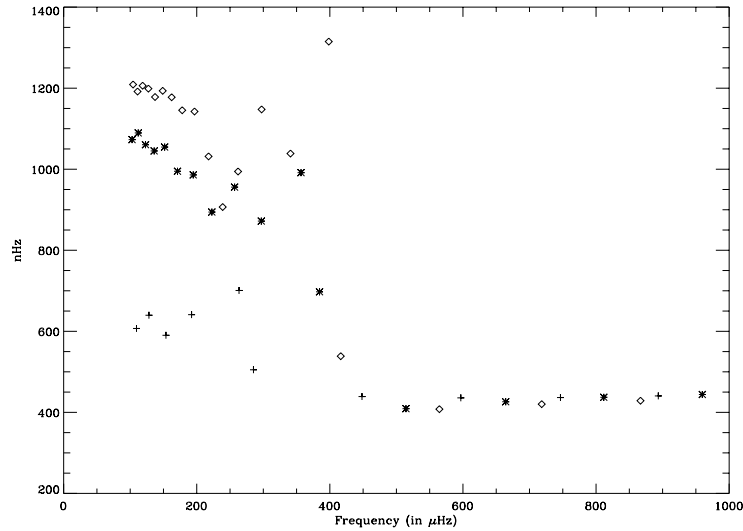


Figure 10: Splitting as a function of frequency for different degree (plus  $l = 1$ , star  $l = 2$ , diamond  $l = 3$ . Core rotation is 1732 nHz.

## 5.2 How low can we go: power sliding strategies

These strategies aimed at detecting lower frequency p modes. At the time of the 2nd workshop, various ideas were blossoming. The main idea was to use theoretical models to look for low frequency p modes. Using these aids to detect these modes would obviously have a small impact on the ‘observed’ solar model.

## 5.3 Detection limit of these p modes

For computing the time needed to detect a given  $n$  mode, we need to know the background noise, the amplitude of the mode and its linewidth. As for the latter, the paper we published in Boston (Fröhlich et al, 1998) gives for the linewidth the mean power law as follows:

$$\Gamma = 0.1 \left( \frac{\nu}{\nu_{\Gamma}} \right)^7. \quad (5)$$

where  $\Gamma$  is the mode linewidth,  $\nu$  is the frequency in mHz and  $\nu_{\Gamma}$  is the reference frequency, 1.600 mHz. Most of the modes at low frequency, say

below 1100  $\mu\text{Hz}$  will not be resolved before a decade or so.

Already with the time series we have (2-3 years long) we cannot resolve modes below 1200  $\mu\text{Hz}$ . It means that with such narrow linewidth, longer time series are likely to help us detect low frequency p modes. We took after Chaplin et al. (1998) (MNRAS, 298, L7) the amplitude dependence (i.e. the total power under the profile) which is given as:

$$A_p = 25 \left( \frac{\nu}{\nu_A} \right)^{7.83} \quad (6)$$

where  $A_p$  is the total power and  $\nu_A$  is the reference frequency, 2.230 mHz. This dependence was derived for mode frequency between 1.680 mHz and 2.230 mHz. This will be used for extrapolating below 1.680 mHz.

Below 1.5 mHz down to 0.1 mHz, the solar background in velocity varies like:

$$B = 0.4 \left( \frac{\nu}{\nu_0} \right)^{-0.8} \quad (7)$$

where  $B$  is in  $(\text{cm/s})^2/\mu\text{Hz}$ ,  $\nu$  is the frequency in  $\mu\text{Hz}$ ,  $\nu_0$  is the reference frequency, 1 mHz.

Therefore the time needed  $T_{det}$  (in years) for detecting low frequency p modes with a given detection level  $\sigma_{det} = 10$  is given by:

$$T_{det} = \frac{2\sigma_{det}B}{A_p} = 5.4\nu^{-8.63} \quad (8)$$

During the last meeting, we detected modes with a signal-to-noise ratio smaller than 10 at 1200  $\mu\text{Hz}$  with a 2-year time series (The formula above would give 1.1 years!). For detecting modes at 1000  $\mu\text{Hz}$ , from the formula above we would get 5.4 years. Clearly we have not detected mode at this frequency range which means that our p-mode amplitude frequency dependence is not so bad after all. So this simple formula explain why it is so difficult to go below the magical frequency of 1 mHz.

## 5.4 Occurrence of 2 visible modes in an $l = 1$ mode

This section was derived after the writing of Douglas. The formula have been significantly corrected but the spirit was kept. The following computation tries to determine the probability to see only a pair of mode in an  $l = 1$  mode,

since it seems sometimes that not all modes can be visible in an  $(m, \nu)$  spectra of MDI.

We assume that the statistical distribution of the power spectra is a  $\chi^2$  with 2 dof. The probability  $p$  of having a peak due to noise above a given detection level  $x_i$  for mode  $i$  is given by:

$$p = e^{-x_i/\langle p \rangle} \quad (9)$$

where  $\langle p \rangle$  is the mean power in a frequency bin where the mode  $i$  is located, i.e  $\langle p \rangle = \langle A \rangle + \langle B \rangle$  where  $\langle A \rangle$  is the amplitude of the mode in the power spectra and  $\langle B \rangle$  is the background noise. If we express  $x_i$  in unit of this background noise as  $\alpha$  we can rewrite the previous expression as a function of the signal-to-noise ratio as:

$$p = e^{-\alpha/(S/N+1)} \quad (10)$$

This simple expression shows that when the modes are detected with a very high S/N, the probability of detection above some level is close to 1. Of course when the S/N is low, the probability of detection is zero. These are 2 very obvious deductions...

Then the probability of seeing a pair of peaks in an  $l = 1$  spectra for mode  $i$  is given by:

$$P_i = 3p^2(1 - p) \quad (11)$$

Then the probability of never seeing one pair for any mode is given by:

$$P_{tot} = \prod_i (1 - P_i) \quad (12)$$

Then the probability of seeing at least one pair is given by:

$$P_{pair} = 1 - \prod_i (1 - P_i) = 1 - \prod_i (1 - 3(1 - e^{-x_i})e^{-2x_i}) \quad (13)$$

The signal-to-noise ratio can be deduced from the previous section as :

$$S/N = 1.77T\nu^{8.6} \quad (14)$$

where  $T$  is in years and  $\nu$  in mHz. Figure 11 shows the probability of seeing a pair of peaks in an  $l = 1$  spectra, deduced from Eq. 11 and 14. The probability of detecting at least one pair given by Eq. 13 is about typically 0.8. We

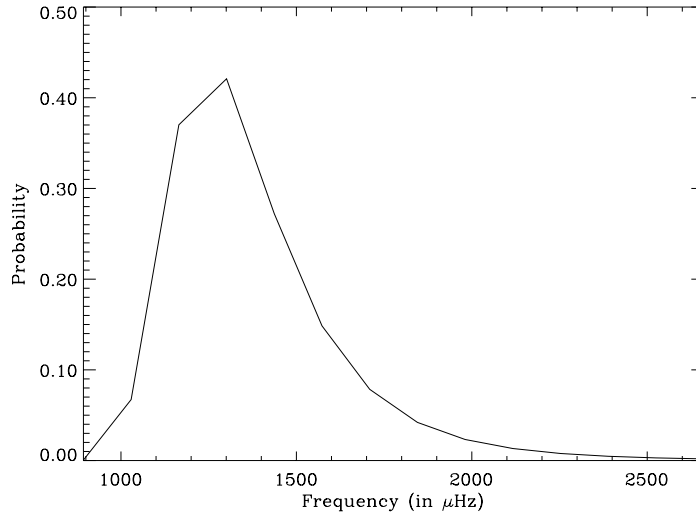


Figure 11: Probability of seeing a pair of peaks in an  $l = 1$  spectra as a function of mode frequency. The detection level  $\alpha = 10$  and the observing time is 2 years. The probability of seeing at least one pair in this range can be deduced from this graph using Eq. 13. For this set of parameters it is about 0.8; other set of parameters give roughly similar values.

must point out that the location of maximum probability is right where the double mode mentioned by Appourchaux (1998) in the MDI data is. When the observing time increases, the peak moves down to lower frequency as one can expect. This is a confirmation of D.Gough calculation that a double mode is not indeed a rare occurrence.

## 5.5 Monte-Carlo simulations of a low S/N doublet

These simulations were undertaken in an effort to address the issue of whether the reluctance of the  $m = -1$  component of the  $\ell = 1$ ,  $n = 8$  mode in the MDI spectrum to reveal itself was in any way unusual, given: (i) an assumed stochastic excitation mechanism; (ii) the length of, and S/N in, the data set; and (iii) the probable characteristics, *e.g.*, line width, of the mode.

### 5.5.1 The model

The model which has been applied here to generate artificial  $p$ -mode-like residuals in the time domain is discussed in more detail elsewhere (Chaplin et al., 1997, MNRAS, 287, 51–56).

Assuming the solar  $p$ -modes to be stochastically excited, a simple and appropriate model is a damped, harmonic oscillator, i.e.,

$$\frac{d^2}{dt^2}x(t) + 2\eta\frac{d}{dt}x(t) + \omega_0^2x(t) = A\delta(t - t_0). \quad (15)$$

In the above:  $x(t)$  is the displacement of the oscillator;  $\omega_0$  is its natural angular frequency;  $\eta$  is the damping constant; and  $A$  is the amplitude of the “white” forcing function  $\delta(t - t_0)$ , which is applied to the oscillator at time  $t_0$ . We note here that the imparting of a force to the oscillator via an infinitesimal kick is physically unrealistic – studies of impulsive events at the top of the convection zone appear to indicate that the forcing may be sustained over many seconds.

The oscillator’s displacement,  $x(t)$ , and velocity,  $dx(t)/dt$ , can be derived by taking Laplace transforms of both sides of the oscillator equation. The solution of the equation, and its first derivative can then be applied in the form of an algorithm to produce a synthetic time series of “ $p$ -mode-like” residuals. Here, a time series in  $dx(t)/dt$  is generated for subsequent Fourier analysis.

Given a chosen frequency  $\omega_0$ , and damping rate  $\eta$ , the initial displacement and velocity of the oscillator are chosen at the start of the first excitation ( $x_0$  and  $dx_0/dt$ ). The oscillator is then allowed to “run” according to solutions of the oscillator equation. Here, the simulated data were generated with a cadence of 40s. The simulated mode was then “re-excited” at an interval of every 40-s sample, i.e., giving  $t_{\text{excite}} \ll \tau_{\text{mode}}$ .

At each re-excitation, the final displacement and velocity of the oscillator during the previous excitation are used as initial input values,  $x_0$  and  $dx_0/dt$ , for the next excitation. The amplitudes of each re-excitation are drawn randomly from a normal distribution with a chosen mean value. In addition, the sense of the “kick” provided by the forcing term, i.e., either with or against the current direction of motion of the oscillator along the arbitrary  $x$  axis, is given equal probability, and is chosen by an unbiased random number generator.

### 5.5.2 Construction of the time series

Each time series constructed here consisted of the sectoral components of the  $\ell = 1$  mode only (i.e., simulating a “full-disc” view). The frequency of the oscillator was set at  $1329.6 \mu\text{Hz}$ . The damping constant was fixed according to the FWHM line width  $\Delta\nu$  (i.e.,  $\eta = \pi\Delta\nu$ ) expected at this frequency from a power-law extrapolation at slightly higher  $n$ . (The selected  $\Delta\nu$  was  $26 \text{ nHz}$ .) I assumed a splitting of  $400 \text{ nHz}$  (i.e., for  $\Delta|m| = 1$ ) for the doublet. This is roughly the raw, synodic value that we measure in real data. The frequency of the oscillator used to generate each  $m$  component was therefore fixed by adding or subtracting  $400 \text{ nHz}$ .

Each independently generated  $m$  component was given a random phase shift before being co-added to give the final time series. In addition, a small amount of normally-distributed “white” noise was added in the time domain to give signal-to-noise ratios which were similar to those observed in the MDI spectrum. Once generated, each composite time series – of simulated length 16 months – was Fourier analyzed to give the power spectrum, and various “house-keeping” statistics characterizing the resultant spectrum in the vicinity of the  $\ell = 1$  multiplet were stored to file.

### 5.5.3 Results

In all, 100 independent time series segments were generated. Fig. 12 shows the result of co-adding the resulting power spectra, which were generated *before* the white-noise component was added in the time domain. Were more such spectra to be co-added, the resulting summation would tend to the Lorentzian limit expected for this model.

Fig. 13 displays an example of an individual power spectrum: the left-hand plot is the spectrum generated from the pure mode, without the addition of noise in the time domain; while the right-hand plot shows the spectrum generated with the white-noise component added in the time domain.

In order to assess whether or not the mode would be detectable in a given spectrum, we use the 1/10th probability criteria. That is: over a reasonable range – say  $100 \mu\text{Hz}$  – what S/N is required in a peak for there to be only a 10-per-cent chance of it appearing by chance (assuming a Boltzmann distribution of powers in the frequency domain)? For the resolution in a 16-month spectrum, the required S/N – which we take to be the maximum height in

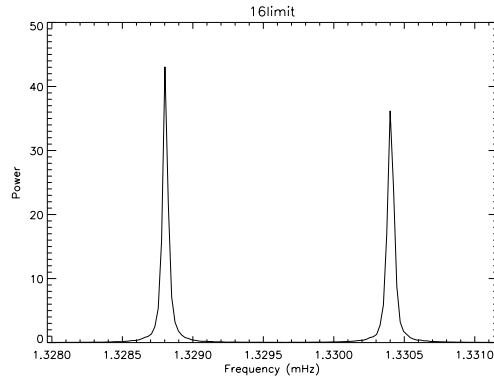


Figure 12: The result of co-adding 100 independent realizations of a simulated  $\ell = 1$  doublet at  $n = 8$ . Here, power spectra generated *without* the addition of white noise in the time domain have been used.

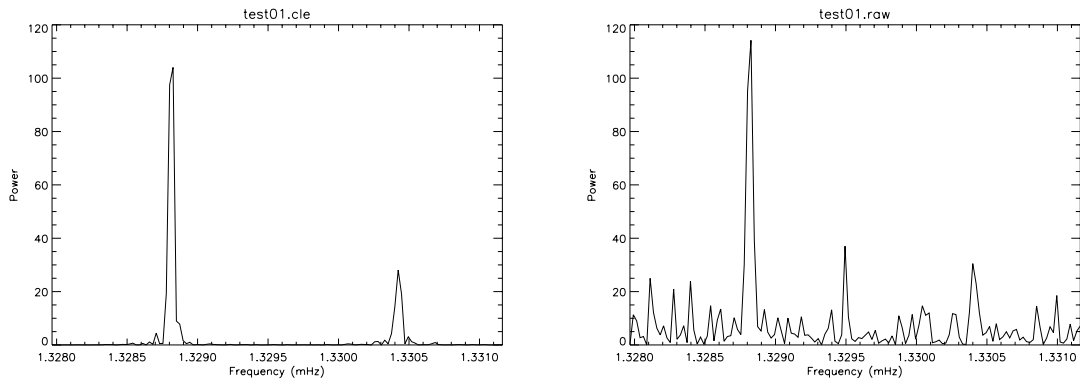


Figure 13: An example of an individual power spectrum. Left-hand plot – spectrum generated from the pure mode, without the addition of noise in the time domain. Right-hand plot – spectrum generated with white noise added in the time domain.

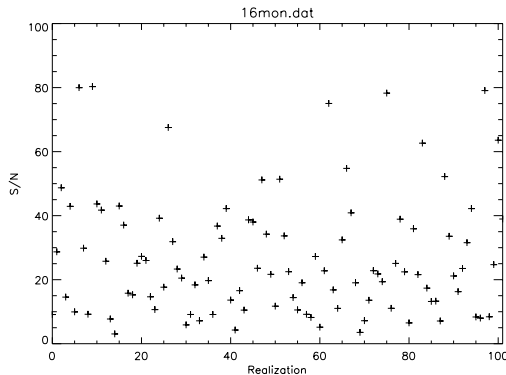


Figure 14: The observed S/N – for the lower-frequency modal component – for each of the 100 independent simulated spectra.

the peak, divided by the  $1\sigma$  power level of the spectrum over the investigated range – is  $\sim 10.6$ . Fig. 14 shows the observed S/N for the lower-frequency component of the simulated  $\ell = 1$  mode in each of the 100 generated realizations.

Form the 100 simulations – admittedly a somewhat restricted population from which to draw any definitive conclusions regarding probabilities – one finds that one or other of the sectoral components lies below the 1/10th threshold about 20 per cent of the time. Further, the chances of one of the components lying above the threshold, while the other lies below it, are about 40 per cent. On only 2 out of the 100 simulations did *both* components lie below the threshold.

So, I think one can conclude that, given the S/N in the data and the assumed nature of the excitation, the appearance of the  $\ell = 1, n = 8$  mode in the MDI spectrum is not that unexpected.

## 6 p-mode amplitude and noise levels

### 6.1 Scale on the ordinate of the GOLF spectrum – comparison with 32-month BiSON spectrum

In order to facilitate proper mode-power and noise-power comparisons between frequency spectra generated by different analyses of different data,

one must be sure about the scaling used on the ordinate. This briefly summarizes how the scaling was deduced for the 2-year GOLF spectrum shown in the SOHO6/GONG'98 conference proceedings; In addition, I give mean power levels and a rough detection threshold for the 32-month BiSON spectrum. I have also taken the opportunity to indulge myself – for the sake of completeness – with a few general comments about scaling. This is where I begin.

### 6.1.1 Mean-square (MS) and Power-Spectral-Density (PSD) scaling

Here, I consider scalings where power in the time domain appears only in the real-frequency side of the FFT – this is often referred to as a “single-sided” transform. The mean-square (MS) scaling is nicely illustrated by considering the power spectrum one expects from a normally distributed noise source in the time domain. Let the sample standard deviation of the “white” noise source be  $\sigma$ . Its magnitude is determined by the distribution of noise-source velocities  $v_i$ : for  $N$  points in the time series

$$\sigma^2 = \sum_{i=1}^N (v_i - \bar{v})^2 / (N - 1).$$

If the time series of white noise possesses a zero mean level, then for  $N \gg 1$ , the right-hand side of the above is simply the sum of the powers  $P_i$  in each real bin of the frequency domain of the Fourier transform of the data. Therefore, the average power per bin in the frequency domain – due to the Gaussian noise source – is given by

$$\sum_{i=1}^{N/2} P_i / (N/2) = \sigma^2 / (N/2).$$

(Note the factor  $N/2$ , *i.e.*, all power appears in the real side of the transform.)  
So:

- The mean power per bin is  $P_{\text{MS}} = \sigma^2 / (N/2)$  – this I refer to as a Mean-Square (MS) scaling.

- Let  $t$  be the sampling cadence of the data, such that the total length of the time series is  $T = Nt$ . Each bin in the frequency domain will have width  $1/Nt$ . Therefore, the mean power per Hz will be given by:

$$P_{\text{PSD}} = \frac{\sigma^2/(N/2)}{1/Nt} = 2\sigma^2 \cdot t.$$

This is what I refer to as Power-Spectral-Density (PSD) scaling.

If the time series consists of several breaks in the data stream, such that the fractional duty cycle is  $\mathcal{F}$ , then the above expressions must be modified to correct for the missing power. They will now be:

$$P_{\text{MS}} = (\sigma^2/(N/2))/\mathcal{F},$$

and

$$P_{\text{PSD}} = 2 \cdot \sigma^2 \cdot t/\mathcal{F}.$$

Now consider a sine wave – with zero-to-peak amplitude  $A$  – forced through a time series. If  $\mathcal{F} = 1$ , the MS scaling will recover a height  $h_{\text{MS}} = A^2/2$ .

### 6.1.2 Equivalent-Sine-Wave (ESW) Scaling

Consider a periodic signal forced through a time series with diurnal breaks. Let the height of the peak in the power spectrum – given a Mean-Square (MS) scaling – again be  $h_{\text{MS}}$ . Now, since power will be re-distributed into the first diurnal sidelobes and their higher harmonics, this will actually underestimate the true power in the signal. If  $A$  is the signal’s true, zero-to-peak amplitude, then the true “mean-square” power we would expect is  $A^2/2$ . The degree to which  $h_{\text{MS}}$  underestimates this will depend upon the fill, *i.e.*,

$$h_{\text{MS}} = \mathcal{F} \cdot A^2/2.$$

So, in order to get a proper estimate of the “true” power in the signal – an Equivalent-Sine-Wave (ESW) scaling – we must correct for the fill twice (*i.e.*, once more than for the MS and PSD scaling). We can use either a zero-to-peak or mean-square ESW scaling. The mean-square ESW scaling is defined according to:

$$P_{\text{ESW}}^{\text{ms}} = P_{\text{MS}}/\mathcal{F} = A^2/2,$$

while the zero-to-peak ESW scaling is defined by:

$$P_{\text{ESW}}^{\text{pp}} = 2P_{\text{MS}}/\mathcal{F} = A^2.$$

Clearly, for  $\mathcal{F} = 1$ ,  $P_{\text{ESW}}^{\text{ms}} = P_{\text{MS}}$ .

### 6.1.3 Scaling in the GOLF spectrum

Here, we refer to the low-frequency analysis of a 2-year GOLF power spectrum presented in the proceedings of the SOHO6/GONG '98 Workshop (Gabriel *et al.*, pp. 61–66). There is sufficient information given to allow one to deduce that a MS scaling has been employed on the ordinate of the spectrum shown in Fig. 2 of the paper.

Here, seven sine waves of slightly different frequency, but the same zero-to-peak amplitude of  $A = 0.8 \text{ cm s}^{-1}$ , have been injected into the GOLF time series. The resulting signals have peak powers in the range  $\sim 1100$  to  $\sim 2800 \text{ m}^2 \text{ s}^{-2} \text{ Hz}^{-1}$ . Given the frequency resolution appropriate to a two-year spectrum, these correspond to powers of  $\sim 0.44$  and  $\sim 0.17 \text{ cm}^2 \text{ s}^{-2}$  per bin. For these levels to be consistent with the statement:

...All 7 [*peaks*] can be clearly seen in the spectrum, but with a dispersion of velocities, between  $0.6$  and  $1.0 \text{ cm s}^{-1}$ ...

the spectrum must be scaled to give  $A^2/2$ , *i.e.*, it is MS scaled. (A MS power level of  $\sim 0.17 \text{ m}^2 \text{ s}^{-2}$  gives  $A \sim 0.6 \text{ mm s}^{-1}$ ; while  $\sim 0.44 \text{ m}^2 \text{ s}^{-2}$  gives  $A \sim 1.0 \text{ mm s}^{-1}$ .)

A crude estimate of the  $1\sigma$  power level in the GOLF spectrum – for the presented range of  $225$  to  $235 \mu\text{Hz}$  – is about  $\sim 150 \text{ m}^2 \text{ s}^{-2} \text{ Hz}^{-1}$ . This gives a  $10\sigma$  threshold for  $A$  of  $\sim 7 \text{ mm s}^{-1}$ .

### 6.1.4 Power levels in the 32-month BiSON spectrum

In addition to the 60-s cadence BiSON time series placed on the OSLO account, I have also generated a 32-month, 40-s-cadence time series that is optimized for the low-frequency range (*i.e.*, for  $200$  to  $1000 \mu\text{Hz}$ ).

A fair question to ask here would be: what do you mean by “optimized for 200 to 1000  $\mu\text{Hz}$ ”? In a time series constructed from data collected at several sites, the spectral noise performance characteristics of the collected data will differ, both between sites and with time, *e.g.*, due to variations in instrumental performance. If there is a noticeable frequency dependence, then the data collected from certain network sites may be better suited to, say, the study of low-frequency phenomena, than those collected at others.

This clearly prompts the question: in order to generate the highest-quality power spectrum over a certain frequency range, which data should be used and which rejected when constructing the corresponding time series? Clearly, this demands data selection criteria that take into account the targeted frequency range of a particular study, and the corresponding quality of the observations made at each site over this range. The need to maximize the duty cycle of the network implies that data should be used, where available, from a given station. However, there is a trade-off between: (i) the introduction of these data to the final data set; and (ii) the possibility that – if they are of poor quality – their use may drive up the noise power level of the combined network set to such an extent that this negates the apparent advantage of using the data in the first place. I have used a formalism that encapsulates the above in a quantitative manner to make (hopefully!) sensible choices about which data to keep in order to build the best time series from the available data.

Here, I ask: (i) what is the mean power level near 220  $\mu\text{Hz}$  in the 32-month BiSON spectrum, where one of the tentative GOLF detections lies; and (ii) would the 0.8-centimetre-per-second sine waves injected into the GOLF time series be detectable in the BiSON spectrum, were the same procedure to be followed?

The  $1\sigma$  level between 218 and 222  $\mu\text{Hz}$  in the BiSON spectrum is  $\sim 0.03 \text{ cm}^2 \text{ s}^{-2}$  per bin (MS scaling). Now, if we inject a sine wave with amplitude  $A$ , we expect – for a commensurate signal – to recover  $\mathcal{F}A^2/2$  (see Section 6.1.2). To get the optimum trade off (see above) for this frequency range, I chose to neglect a not-insubstantial fraction of available data – this left a duty cycle for the 32-month BiSON time series of about 60 per cent. So, we would expect our commensurate sine wave to give a peak with height  $\sim 0.19 \text{ cm}^2 \text{ s}^{-2}$  per bin in our MS-scaled spectrum. This corresponds to a S/N of about  $\sim 7$ .

To reach the  $10\sigma$  level would require a signal of amplitude  $A \sim 10 \text{ mm s}^{-1}$ .

So, we conclude that, very roughly, an upper limit to the detection threshold from this 32-month BiSON spectrum is about  $\sim 10 \text{ mm s}^{-1}$ . Were the duty cycle of the time series to have been 100 per cent – with data of similar quality – this would have been reduced to about  $\sim 8 \text{ mm s}^{-1}$ .

## 6.2 Scale in the MDI spectrum

The scaling of the MDI data seemed to have been correctly done as we can judge from the Fröhlich et al paper published in Boston. ThierryA performed the scaling using the amplitude A as the output. The scaling performed by ThierryT is yet to be known.

## 6.3 Noise level in GOLF

According to paper by Henney et al (1999) (submitted to A&A) , it seems that the level computed in the previous agrees with the computation of GOLF, i.e. about about  $\sim 150 \text{ m}^2 \text{ s}^{-2} \text{ Hz}^{-1}$  in the range 225 to 235  $\mu\text{Hz}$ .

## 6.4 Reduction of noise in the MDI data

P.Scherrer invented new techniques for reducing the noise in the spectra. One technique is to follow the solar rotation thereby reducing the effect of granules coming in and coming out of the field. The other technique is to use only the central part of the disk where the super- and meso-granulation noises are smaller than at the limb. The latter technique was tried but did not give any result due to the lack of time; we will try again.

## References

- [TA98] Appourchaux, T., 1998., SOHO 6 Proceedings, p. 37
- [CF84] Fröhlich, C. & Delache, P. 1984, Memorie della Societa Astronomica Italiana, 55, 99

## 7 Appendix B: Mode frequencies

Table 1: Mode frequency for Nice model (S13-I-4406).  $l = 0, 1$

$l$	mode type- $n$	Frequency (in $\mu\text{Hz}$ )	Splitting (in nHz)
0	p1	257.61	
0	p2	403.93	
0	p3	535.38	
0	p4	680.17	
0	p5	825.09	
0	p6	972.59	
0	p7	1118.05	
0	p8	1263.44	
0	p9	1407.59	
0	p10	1548.44	
0	p11	1686.77	
0	p12	1822.23	
0	p13	1957.49	
1	g5	107.67	212.
1	g4	125.96	210.
1	g3	151.26	210.
1	g2	189.00	213.
1	g1	259.75	242.
1	p1	284.21	396.
1	p2	448.31	433.
1	p3	596.84	429.
1	p4	746.56	427.
1	p5	893.63	427.
1	p6	1039.45	428.
1	p7	1185.59	428.
1	p8	1329.69	429.
1	p9	1473.00	430.
1	p10	1612.83	430.
1	p11	1749.48	431.
1	p12	1885.26	431.

Table 2: Mode frequency for Nice model (S13-I-4406).  $l = 2$

$l$	mode type- $n$	Frequency (in $\mu\text{Hz}$ )	Splitting (in nHz)
2	g10	100.97	365.
2	g9	110.12	365.
2	g8	120.85	365.
2	g7	133.68	363.
2	g6	149.29	360.
2	g5	168.36	354.
2	g4	191.70	346.
2	g3	219.75	345.
2	g2	253.54	373.
2	g1	293.89	409.
2	f	352.14	366.
2	p1	382.44	348.
2	p2	514.29	391.
2	p3	664.34	411.
2	p4	811.71	420.
2	p5	959.85	425.
2	p6	1105.12	427.
2	p7	1250.67	430.
2	p8	1394.67	431.
2	p9	1535.91	432.
2	p10	1674.66	433.
2	p11	1810.32	434.
2	p12	1945.89	434.

Table 3: Mode frequency for Nice model (S13-I-4406).  $l = 3$

$l$	mode type- $n$	Frequency (in $\mu\text{Hz}$ )	Splitting (in nHz)
3	g14	102.42	400.
3	g13	109.07	401.
3	g12	116.57	401.
3	g11	125.06	401.
3	g10	134.89	401.
3	g9	146.32	401.
3	g8	159.55	401.
3	g7	175.08	400.
3	g6	193.49	396.
3	g5	214.69	385.
3	g4	236.20	373.
3	g3	258.90	399.
3	g2	293.06	416.
3	g1	336.68	422.
3	f	392.17	406.
3	p1	415.66	384.
3	p2	564.60	403.
3	p3	718.47	416.
3	p4	866.94	423.
3	p5	1015.00	427.
3	p6	1161.72	429.
3	p7	1306.79	432.
3	p8	1451.09	433.
3	p9	1591.56	434.
3	p10	1729.20	436.
3	p11	1865.30	436.
3	p12	2001.16	436.

Table 4: Mode frequency for Nice model (S13-I-4406).  $l = 4$

$l$	mode type- $n$	Frequency (in $\mu\text{Hz}$ )	Splitting (in nHz)
4	g18	102.74	414.
4	g17	107.89	414.
4	g16	113.54	414.
4	g15	119.77	414.
4	g14	126.73	414.
4	g13	134.54	415.
4	g12	143.27	415.
4	g11	153.08	415.
4	g10	164.29	416.
4	g9	177.25	416.
4	g8	192.06	416.
4	g7	209.13	415.
4	g6	228.85	410.
4	g5	248.51	385.
4	g4	262.89	398.
4	g3	288.16	422.
4	g2	324.09	424.
4	g1	364.64	429.
4	f	410.83	420.
4	p1	441.54	397.
4	p2	603.20	414.
4	p3	761.13	423.
4	p4	913.21	427.
4	p5	1062.11	431.
4	p6	1210.60	432.
4	p7	1356.37	434.
4	p8	1500.41	436.
4	p9	1641.00	436.
4	p10	1778.10	437.
4	p11	1914.83	438.

Table 5: Mode frequency for Nice model (S13-I-4406).  $l = 5$

$l$	mode type- $n$	Frequency (in $\mu\text{Hz}$ )	Splitting (in nHz)
5	g22	102.77	420.
5	g21	106.95	420.
5	g20	111.46	420.
5	g19	116.36	421.
5	g18	121.70	421.
5	g17	127.54	421.
5	g16	133.92	421.
5	g15	140.92	421.
5	g14	148.68	421.
5	g13	157.34	422.
5	g12	166.95	422.
5	g11	177.66	422.
5	g10	189.77	423.
5	g9	203.63	423.
5	g8	219.29	423.
5	g7	237.08	422.
5	g6	257.18	417.
5	g5	271.06	380.
5	g4	285.13	422.
5	g3	312.71	427.
5	g2	346.63	428.
5	g1	381.86	431.
5	f	420.57	425.
5	p1	467.75	407.
5	p2	637.84	421.
5	p3	798.92	428.
5	p4	954.33	430.
5	p5	1104.88	433.
5	p6	1254.57	435.
5	p7	1401.64	436.
5	p8	1545.32	437.
5	p9	1685.97	438.
5	p10	1823.40	438.
5	p11	1960.61	439.

Table 6: Mode frequency for Nice model (S13-I-4406).  $l = 6$

$l$	mode type- $n$	Frequency (in $\mu\text{Hz}$ )	Splitting (in nHz)
6	g25	106.23	424.
6	g24	109.99	424.
6	g23	114.00	424.
6	g22	118.31	424.
6	g21	122.96	424.
6	g20	127.95	424.
6	g19	133.35	425.
6	g18	139.21	425.
6	g17	145.60	425.
6	g16	152.55	425.
6	g15	160.13	425.
6	g14	168.48	425.
6	g13	177.73	426.
6	g12	187.93	426.
6	g11	199.20	426.
6	g10	211.82	426.
6	g9	226.13	426.
6	g8	242.11	427.
6	g7	260.04	427.
6	g6	280.09	421.
6	g5	288.25	387.
6	g4	305.29	428.
6	g3	331.93	429.
6	g2	362.97	430.
6	g1	393.00	432.
6	f	426.74	427.
6	p1	493.12	415.
6	p2	670.05	425.
6	p3	834.21	431.
6	p4	992.27	433.
6	p5	1145.00	435.
6	p6	1295.54	437.
6	p7	1443.77	437.
6	p8	1587.46	438.
6	p9	1727.86	439.
6	p10	1866.15	439.

Table 7: Mode frequency for GONG model computed at Nice.  $l = 0, 1$

$l$	mode type- $n$	Frequency (in $\mu\text{Hz}$ )	Splitting (in nHz)
0	p1	258.01	
0	p2	404.48	
0	p3	535.94	
0	p4	680.57	
0	p5	825.36	
0	p6	972.74	
0	p7	1118.15	
0	p8	1263.51	
0	p9	1407.62	
0	p10	1548.51	
0	p11	1686.80	
0	p12	1822.21	
0	p13	1957.45	
1	g5	109.27	214.
1	g4	127.89	212.
1	g3	153.39	211.
1	g2	191.88	214.
1	g1	262.98	253.
1	p1	285.11	385.
1	p2	448.47	433.
1	p3	596.94	429.
1	p4	746.66	427.
1	p5	893.71	427.
1	p6	1039.56	428.
1	p7	1185.62	428.
1	p8	1329.69	429.
1	p9	1472.97	430.
1	p10	1612.72	430.
1	p11	1749.38	431.
1	p12	1885.09	431.

Table 8: Mode frequency for GONG model computed at Nice.  $l = 2$

$l$	mode type- $n$	Frequency (in $\mu\text{Hz}$ )	Splitting (in nHz)
2	g10	102.60	365.
2	g9	111.85	365.
2	g8	122.75	364.
2	g7	135.74	363.
2	g6	151.48	359.
2	g5	170.70	353.
2	g4	194.36	345.
2	g3	222.32	346.
2	g2	256.51	376.
2	g1	296.53	408.
2	f	355.78	361.
2	p1	384.16	352.
2	p2	514.47	391.
2	p3	664.40	411.
2	p4	811.76	420.
2	p5	959.87	425.
2	p6	1105.17	427.
2	p7	1250.72	430.
2	p8	1394.70	431.
2	p9	1535.98	432.
2	p10	1674.67	433.
2	p11	1810.27	434.
2	p12	1945.81	434.

Table 9: Mode frequency for GONG model computed at Nice.  $l = 3$

$l$	mode type- $n$	Frequency (in $\mu\text{Hz}$ )	Splitting (in nHz)
3	g14	104.13	400.
3	g13	110.85	401.
3	g12	118.46	401.
3	g11	127.12	401.
3	g10	137.05	401.
3	g9	148.58	401.
3	g8	162.01	401.
3	g7	177.72	399.
3	g6	196.24	395.
3	g5	217.34	384.
3	g4	238.68	374.
3	g3	261.65	402.
3	g2	296.84	416.
3	g1	340.11	422.
3	f	396.98	403.
3	p1	416.35	386.
3	p2	564.71	403.
3	p3	718.51	416.
3	p4	866.95	423.
3	p5	1015.01	427.
3	p6	1161.69	429.
3	p7	1306.79	432.
3	p8	1451.05	433.
3	p9	1591.54	434.
3	p10	1729.20	436.
3	p11	1865.24	436.
3	p12	2001.08	436.

Table 10: Mode frequency for GONG model computed at Nice.  $l = 4$

$l$	mode type- $n$	Frequency (in $\mu\text{Hz}$ )	Splitting in nHz
4	g18	104.46	414.
4	g17	109.68	414.
4	g16	115.42	414.
4	g15	121.77	414.
4	g14	128.82	415.
4	g13	136.70	415.
4	g12	145.56	415.
4	g11	155.55	415.
4	g10	166.90	416.
4	g9	179.93	416.
4	g8	194.94	416.
4	g7	212.22	414.
4	g6	231.93	408.
4	g5	250.62	382.
4	g4	265.42	404.
4	g3	291.73	422.
4	g2	328.39	424.
4	g1	368.25	429.
4	f	416.24	420.
4	p1	441.66	397.
4	p2	603.23	414.
4	p3	761.14	423.
4	p4	913.17	427.
4	p5	1062.09	431.
4	p6	1210.52	432.
4	p7	1356.29	434.
4	p8	1500.34	436.
4	p9	1640.89	436.
4	p10	1778.01	437.
4	p11	1914.71	438.

Table 11: Mode frequency for GONG model computed at Nice.  $l = 5$

$l$	mode type- $n$	Frequency (in $\mu\text{Hz}$ )	Splitting (in nHz)
5	g22	104.51	420.
5	g21	108.74	420.
5	g20	113.33	420.
5	g19	118.30	421.
5	g18	123.71	421.
5	g17	129.63	421.
5	g16	136.11	421.
5	g15	143.23	421.
5	g14	151.10	421.
5	g13	159.83	422.
5	g12	169.57	422.
5	g11	180.47	422.
5	g10	192.73	423.
5	g9	206.65	423.
5	g8	222.51	423.
5	g7	240.52	422.
5	g6	260.41	413.
5	g5	272.20	383.
5	g4	288.63	424.
5	g3	316.66	427.
5	g2	351.14	428.
5	g1	385.46	431.
5	f	426.19	424.
5	p1	467.80	407.
5	p2	637.83	421.
5	p3	798.90	428.
5	p4	954.25	430.
5	p5	1104.81	433.
5	p6	1254.49	435.
5	p7	1401.51	436.
5	p8	1545.23	437.
5	p9	1685.84	438.
5	p10	1823.21	438.
5	p11	1960.44	439.

Table 12: Mode frequency for GONG model computed at Nice.  $l = 6$

$l$	mode type- $n$	Frequency (in $\mu\text{Hz}$ )	Splitting (in nHz)
6	g25	108.02	424.
6	g24	111.83	424.
6	g23	115.91	424.
6	g22	120.28	424.
6	g21	124.99	424.
6	g20	130.06	424.
6	g19	135.55	425.
6	g17	147.96	425.
6	g16	155.00	425.
6	g15	162.71	425.
6	g14	171.17	425.
6	g13	180.50	425.
6	g12	190.83	426.
6	g10	215.06	426.
6	g9	229.41	426.
6	g8	245.58	427.
6	g7	263.74	427.
6	g6	283.28	427.
6	g5	289.19	413.
6	g4	309.16	395.
6	g3	336.04	428.
6	g2	367.57	429.
6	g1	396.56	430.
6	f	432.52	432.
6	p1	493.15	427.
6	p2	670.02	415.
6	p3	834.18	425.
6	p4	992.18	431.
6	p5	1144.88	433.
6	p6	1295.42	435.
6	p7	1443.61	437.
6	p8	1587.31	437.
6	p9	1727.71	438.
6	p10	1865.91	439.